Energetic, electronic, and magnetic properties of Mn pairs on reconstructed (001) GaAs surfaces

Magdalena Birowska*
Faculty of Physics, University of Warsaw, Pasteura 5, PL-02-093 Warszawa, Poland

Cezary Śliwa
Institute of Physics, Polish Academy of Sciences, al. Lotników 32/46, PL-02-668 Warszawa, Poland

Jacek A. Majewski
Faculty of Physics, University of Warsaw, Pasteura 5, PL-02-093 Warszawa, Poland

(Received 20 October 2016; revised manuscript received 14 February 2017; published 22 March 2017)

We study energetic, magnetic, and electronic properties of diluted substitutional Mn pairs on reconstructed (001) GaAs surfaces. The studies are based on first-principles calculations in the framework of density functional theory. We demonstrate that the stability of the systems strongly depends on the position, orientation, and the distance between the Mn atoms constituting the pair. Independently of the considered surface reconstruction pattern, the Mn pairs with Mn atoms being the nearest neighbors (NN) on a cationic sublattice turn out to be energetically more favorable than the pairs with the larger distance between the Mn atoms. However, the preferential buildup orientation of the Mn-NN pair depends on the surface reconstruction and is parallel to either the [110] or the [1$\bar{1}$0] crystallographic direction. We reveal also the mechanisms of the magnetic ordering of Mn-NN pairs. The Mn-NN pairs along the [110] crystallographic direction exhibit always ferromagnetic alignment of Mn spins, whereas the spins in the Mn-NN pairs along the [1$\bar{1}$0] direction are mostly antiferromagnetically aligned. In the electronic structure of the systems containing Mn pairs with ferromagnetically aligned spins, we observe the valence band hole states in the neighborhood of Fermi energy. This indicates that the surface ferromagnetism in this prototype of dilute magnetic semiconductors can be explained in terms of the *p-d* Zener model.

DOI: 10.1103/PhysRevB.95.115311

I. INTRODUCTION

Nowadays, epitaxially grown semiconducting magnetic films such as (Ga,Mn)As have attracted a great deal of attention, mostly due to their intriguing physical properties, such as magnetocrystalline anisotropy allowing for the control of magnetotransport phenomena [1,2], that make them promising candidates for spintronic applications. The properties of these materials depend strongly on how the magnetic ions are incorporated into the host. For example, it is commonly accepted [1,2] that the interstitial Mn ions in bulk GaAs reduce the concentration of holes in the valence band, and hence diminish the Curie temperature and hinder *p-d* Zener-type ferromagnetism. On the other hand, it was predicted [3] that interstitial Mn ions might induce a new type of ferromagnetism in Mn-doped GaAs through formation of the substitutional-interstitial Mn complexes. Moreover, it has been demonstrated by the authors [4] that the bulk uniaxial, in-plane and out-of-plane, magnetic anisotropies originate from the existence of the preferential buildup direction of the Mn atoms being the nearest neighbors along a crystallographic direction. This preferential buildup direction of Mn atoms has been ascribed to the growth mechanism of (Ga,Mn)As and the manner in which the Mn pairs are incorporated into the (001) GaAs surface during the growth process [4].

Since the uniaxial magnetic anisotropy in these dilute magnetic semiconductors (DMSs) is of crucial importance for the design of novel spintronics devices based on these systems [5], the deep physical understanding of its origins and also finding out the mechanisms that allow for tuning the anisotropy through the suitable choice of growth conditions are worth further studies. Furthermore, it has been recently reported that a single atom substitution technique together with spectroscopic imaging in a scanning tunneling microscope (STM) open a new way to manipulate atom by atom at the surface [6] and, therefore, the surface magnetism. In the present studies, we employ *ab initio* calculations in the framework of density functional theory (DFT) to address the following issues: (i) the energetics of the Mn pair substituted into the cationic sublattice on various reconstructed (001) GaAs surfaces, (ii) the influence of the local environment on relative orientation of localized spins of Mn atoms and the induced type of surface magnetism, (iii) the determination of the exchange constants for Mn-Mn interactions in spin Hamiltonians, and (iv) the changes of the surface electronic structure induced by the incorporated Mn atoms. We aim to study the interactions between two Mn atoms unaffected by the presence of the other magnetic atoms, so we consider the lowest computationally tractable Mn coverage of the surface (12.5%), which corresponds roughly to the highest Mn concentration in the synthesized (Ga:Mn)As bulks [1,2]. To determine the physical model for our studies, we have made use of findings reported on the basis of previous DFT calculations for GaAs bulk doped with Mn [3], and scanning tunneling microscopy (STM) measurements supported by DFT calculations for Mn-covered surfaces [7–9]. Before we point out the results of those studies most relevant for us, we would like to mention the empirical studies (in the framework of the self-consistent Hückel method and cluster model) showing that the Mn atoms prefer to be substituted at the surface Ga atoms instead of being adsorbed above them

*Magdalena.Birowska@fuw.edu.pl

[10]. The deposition of Mn onto the GaAs surfaces happens mostly in the As-rich growth conditions. In this case, according to the Ref. [3], the Mn atoms preferentially substitute Ga atoms in the cationic sublattice of GaAs bulk rather than build in the interstitial sites. The similar preference of the cation substitutional over interstitial position under As-rich conditions was predicted for isolated Mn atoms on the (001) GaAs surface in the DFT calculations [7]. Also in Ref. [9], it was predicted in the DFT calculations that under As-rich conditions Mn atoms are favorably incorporated into Ga sites at the $c(4 \times 4)$ reconstructed (001) GaAs surface with Mn coverage of 1/4 mono-layer (ML). The DFT calculations in Ref. [9] were motivated by the STM experiments reported therein, which demonstrated that reconstruction of the Mn-covered surface changes with the growth temperature. The experiments indicated also the existence of the (2×2) types of reconstructions. The Mn-induced surface reconstructions were also studied both by STM and DFT calculations for higher than 1/4 Mn coverage, namely for Mn coverage of 1/2 ML, 3/4 ML, and 1 ML [8]. The STM images revealed also the coexisting areas of 2×2 and 2×4 reconstructions on As-terminated (001) GaAs surface covered with Mn [8]. The DFT calculations indicated that the 2×4 reconstructions should be preferential for lower Mn coverage [8]. In spite of the fact that the experimental and theoretical studies of Mn-covered (001) GaAs surfaces [7,8] were performed for higher Mn coverage than considered in this paper, they clearly indicate the importance of the 2×4 reconstructions and the fact that in As-rich conditions the Mn atoms substitute Ga atoms. Therefore, to get an overall understanding of the incorporation mechanisms of the isolated Mn pairs on the (001) GaAs surface, and facilitate comparison between various surface geometries, we have performed extensive studies of all possible nonequivalent substitutional positions of the Mn pairs onto (001) reconstructed GaAs surfaces—(2×1), $\beta(2 \times 4)$, $\beta 2(2 \times 4)$—under As-rich conditions, employing the identical computational tool. In contrast to calculations reported in Refs. [7,8], where only the standard approximations to the DFT were employed, we decided to perform calculations also within the L(S)DA+U procedure [11,12], which proved to lead to better agreement with experimental results for bulk DMSs [1,2], in addition to the standard L(S)DA approximation. Therefore, the present studies constitute a complement to the previous ones [7,8] concerning the stability and morphology of the Mn-covered reconstructed (001) GaAs surfaces and provide knowledge of physical mechanisms that determine the magnetic interactions between two Mn atoms at the (001) GaAs surfaces.

The magnetic interactions of Mn ions on GaAs surfaces of various orientations are only very weakly understood up to now. Strandberg *et al.* [13] studied the Mn pairs at different crystallographic orientations on the (110) GaAs surface by employing the kinetic tight-binding model. They showed that the long-range interactions were anisotropic in terms of orientations and distances between the Mn pairs. They also demonstrated that the magnetic ions prefer to be ferromagnetically arranged. The anisotropic character of the effective exchange constant for the Mn pairs differently oriented at the (110) surface has been shown in Ref. [14], by using the density functional method. In these two papers, the most common cleaved surface employed in cross-sectional STM studies has been considered, albeit it is not the most common GaAs growth surface [which is the (001) one]. In the literature, there is lack of information about the exchange interaction between the magnetic ions (particularly in dilute regime) placed onto the experimentally observed reconstructed (001) GaAs surfaces.

Detailed knowledge of the magnetic interactions at the reconstructed surfaces is essential for fabricating new high speed spintronics devices. Therefore, in this work we investigate magnetic properties of Mn pairs incorporated into the differently reconstructed (001) GaAs surfaces in the diluted case. Moreover, we report the role of the surface reconstruction in the energetics of the Mn incorporation process and stability of the Mn-GaAs surfaces.

The main objective of the present paper is to study the stability, magnetic interactions, and electronic structure of isolated Mn pairs incorporated into reconstructed (001) GaAs surfaces. This should allow us also to deepen the understanding of the relation between the preferential distribution of the Mn pairs incorporated into the GaAs and the uniaxial magnetic anisotropy, which has been recently demonstrated [4]. The separated Mn pairs have been chosen, since it is known that Mn atoms in GaAs have a tendency to cluster [15], and there are some experimental suggestions that such Mn pairs can really form in some growth conditions as described in Ref. [4]. We note that according to Ref. [16] the Mn ions forming pairs occupy Ga substitutional positions, and once formed, they remain stable through the further growth process as well as during postgrowth annealing at low temperatures $T_a < T_g$ which are employed to diffuse out Mn in interstitial positions. Of course, such effects as the existence of single Mn atoms at the surface, interaction of the Mn atoms with various types of surface structural defects, and/or disorder of Mn pairs would correspond probably to more realistic situations to be encountered in a growth process; however, such studies seem to lie outside the scope of *ab initio* calculations at present. Nevertheless, we believe that our studies shed light on the mechanisms of stability and mutual magnetic interactions between Mn atoms at surfaces. This has particular importance in times when individual atoms can be placed at surfaces employing direct techniques such as STM, for example.

The paper is organized as follows. In Sec. II, we present computational details. The results are presented and discussed in Sec. III. Here we deal with the morphology, energetics, magnetic interactions, and electronic structure of the Mn pairs on the reconstructed (001) GaAs surfaces. Finally, the paper is concluded in Sec. IV.

II. COMPUTATIONAL DETAILS

The calculations are performed within the DFT [17,18] computational scheme employing the L(S)DA+U approach and parametrization of the exchange-correlation functional provided by Ceperly and Adler (CA) [19], as implemented in the SIESTA code [20]. The electron ion-core interactions are represented by norm-conserving pseudopotentials of the Troullier-Martins type [21] with nonlinear core corrections [22]. The electron wave functions are expanded into a flexible multiple centered atom basis set of numerical atomic orbitals

[23]. In the calculations we use double-ζ for the s and p shells of any element and a triple-ζ basis set for the Mn $3d$ shell. The cutoff of 300 Ry is used for the real-space mesh. The Brillouin zone (BZ) integration is performed by means of the k-grid parameter of 30 Å, which corresponds to 16 k points in the full Brillouin zone on the $(4 \times 4 \times 2)$ shifted k grid. For the L(S)DA+U calculations, we adopted the value of the U parameter equal to 4.5 eV for Mn $3d$ states, which is in perfect agreement with the previous photoemission data [24], and consistent with previous L(S)DA+U calculations for the bulk [12,25].

The important issue of large-scale computations is to evaluate their internal accuracy. In particular, we are interested in energetics of the surface calculations; therefore, the convergence of the surface free energy is systematically checked. We have essentially four parameters that determine the internal accuracy (or convergence) of the computations, i.e., the accuracy of computations for chosen density functional and pseudopotentials. These parameters are (i) kinetic energy cutoff, or in the SIESTA code the cutoff for the real space, (ii) the number of k points, or in the SIESTA code the so-called k-grid parameter, (iii) the number of layers in the slab, and (iv) width of the vacuum region in the supercell. The first two parameters have been defined above, and the other two will be determined later on, just describing the geometry of the system. We have tested the convergence of the surface energy with respect to all four parameters. We increased the value of one parameter systematically, simultaneously keeping the other three constant, and observed the convergence of the surface energy. Within this procedure, we estimated the surface energy convergence error connected to the employed k-point grid to be of the order of 0.05 meV/Å^2. Similarly, the chosen cutoff for the real-space mesh leads to the estimated error in the surface free energy of the order of 0.07 meV/Å^2. In a similar manner we estimate the convergence errors in the surface free energy connected to the width of the vacuum layer and the number of layers in the slab. Altogether, the estimated internal accuracy of calculations of the surface free energy (being the sum of four errors) is not smaller than 0.37 meV/Å^2, which is quite accurate, if one compares this value with the typical values of the (001) GaAs surface energies [26], lying in the range 40 to 100 meV/Å^2.

Model of a surface

In order to investigate the physical properties of substitutional isolated Mn pairs on the GaAs(001) surfaces, we used supercell geometry and construct the slab system as it is presented in Fig. 1. To model the (001) GaAs surface, 8 double As-Ga layers (DLs) lying in the (001) crystallographic planes are used. The GaAs crystal is represented by a standard zinc blende (zb) cell with the calculated lattice parameter equal to 5.639 Å, which is in good agreement with experimental value of 5.648 Å [27]. If the slab is not thick enough, the dangling bond states on the two sides of the slab might interact with each other and give rise to artificial charge transfer from the top surface of the slab to its bottom. To avoid this effect and decouple the two sides of the slab, we saturate the dangling bonds from the bottom side of the slab by a monolayer of pseudo-hydrogen-atoms with fractional charge

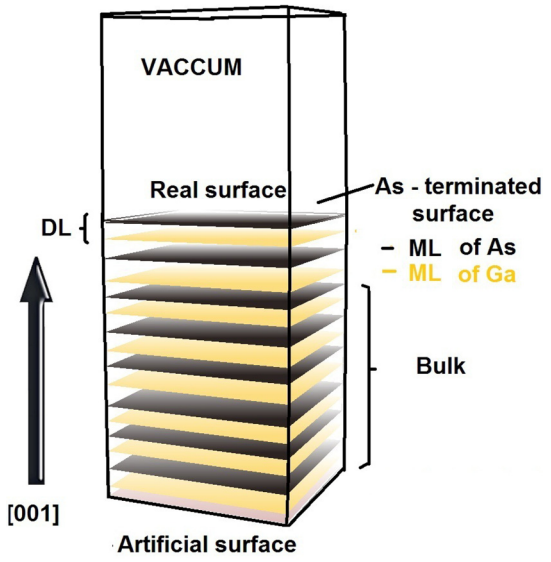

FIG. 1. The schematic diagram of the supercell used in the calculations. The supercell consists of 8 double layers of As-Ga. Each monolayer contains 16 atoms. The artificial surface denotes the surface with hydrogen-saturated dangling bonds of the Ga ML, which mimics the bulk type of bindings.

equal to $Z = 1.25$. Each of the Ga atoms is saturated by two pseudoatoms, to mimic the bulk types of bonds. In order to simulate the independent crystal surface, 16 Å of vacuum is added (it corresponds to 12 MLs of the bulk crystal), with the slab dipole correction option enabled, as implemented in the SIESTA code [20].

We consider experimentally observed reconstructed (001) GaAs surfaces under As-rich conditions: $\beta(2 \times 4)$ [28], $\beta 2(2 \times 4)$ [29–32], and also a theoretically proposed (2×1) reconstruction [33,34], which are presented in Fig. 2. All of the atoms in pure surfaces are fully relaxed until the maximal force on each atom reaches the value of 0.02 eV/Å. These surfaces are our starting points for further calculations.

To investigate the physical properties of isolated Mn pairs (modeling the properly diluted case), we substitute two Ga atoms with two Mn atoms at the topmost monolayer of Ga atoms at pure (001) GaAs reconstructed surfaces. Our simulated supercells contain 288 atoms for (2×1), 284 atoms for $\beta(2 \times 4)$, and 276 atoms for $\beta 2(2 \times 4)$ reconstructed surfaces. Each monolayer comprises 16 atoms, making the Mn coverage of the layer equal to 1/8. The surface area corresponds to the lateral (4×4) cell of dimensions 16 Å $\times$ 16 Å. During the optimization procedure, six MLs from the top of the slab are fully relaxed, whereas the bottom of the slab is fixed to reflect the bulk character of this part of the supercell.

III. RESULTS

Here we present the main results of our studies. First, we describe the energetic issues in Sec. III A, and then we turn to the electronic and magnetic properties of the surfaces with incorporated Mn pairs in Sec. III B.

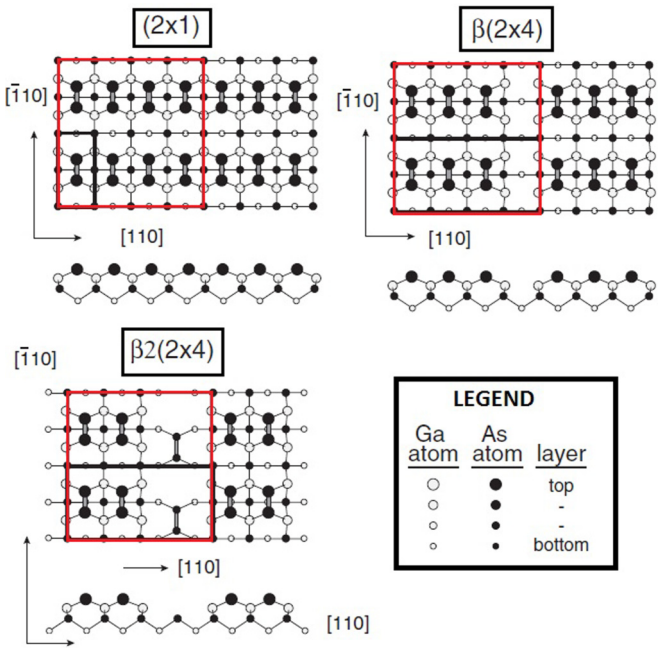

FIG. 2. The top-view and side-view schematic diagrams of (001) GaAs reconstructed surfaces under As-rich conditions used in this work. On the surface, As-As dimerization along the $[\bar{1}10]$ direction is clearly visible. Four monolayers from the top of the slab are shown. Positions in the uppermost atomic layers are indicated by larger symbols. The black and white balls indicate the arsenic and gallium atoms, respectively. The rectangular, red line denotes the lateral supercell chosen for the calculations.

A. Energetics

In this section, we focus on structural and energetic properties from the standpoint of the different possible incorporations of Mn pairs which are embedded onto a cationic sublattice into the three reconstructed (001) GaAs surfaces: (2×1), $\beta(2 \times 4)$, and $\beta 2(2 \times 4)$.

We discuss first each of the reconstructed surfaces, and then provide a comparison between the three studied reconstructions.

1. Reconstruction (2 × 1)

We start the discussion of energetics of the Mn pair incorporated at the (001) GaAs surfaces with the case of the (2×1) surface reconstruction. We treat this case as a prototype and describe the methodology used to study Mn pairs on other reconstructed surfaces. Two Mn atoms can be substituted on Ga sites of the 4×4 lateral unit cell (see Fig. 2) in many ways as indicated in Fig. 3. We consider substitution of Mn atoms into the second from the top cationic (Ga) layer (the top layer consists of As atoms); i.e., for all considered configurations the Mn pairs lie in the (001) crystallographic plane. The first Mn atom is substituted on the Ga site indicated as "0", Mn(0). The possible position of the second Mn atom is indicated by the crystallographic direction along which the pair can be placed $[kl0]$ and the integer n ($n = 1,2,3,\ldots$) that indexes possible positions of the second Mn along this direction. The configuration of the Mn(0)-Mn(n) pair along the $[kl0]$ direction will be indicated as 0-n $[kl0]$ from now on. As seen in Fig. 3, there are three possible configurations of the Mn pair along the $[1\bar{1}0]$ direction, but only two along the [110] and [100] directions, and only one Mn pair configuration along the [310], $[5\bar{1}0]$, $[3\bar{1}0]$, and $[2\bar{1}0]$ directions. Because of the periodic boundary conditions imposed on the lateral supercell, some of the indicated possible Mn positions are equivalent; specifically, the Mn(0)-Mn(3) pair is equivalent to the Mn(1)-Mn(2) pair. Altogether, one has 11 nonequivalent Mn pairs in the 4×4 lateral unit cell of the (2×1) reconstructed surface: three with Mn atoms being nearest neighbors on the cationic sublattice (indicated as 0-1 $[1\bar{1}0]$, 0-1 [110], 0-3 $[1\bar{1}0]$) with the Mn-Mn distances $R = 3.46$ Å, $R = 3.81$ Å, and $R = 4.41$ Å, respectively; two with Mn atoms being the second-nearest neighbors (0-1 [100], 0-1 $[2\bar{1}0]$), $R = 5.34$ Å and $R = 5.95$ Å, respectively; two with Mn atoms being the third-nearest neighbors (0-2 $[1\bar{1}0]$, 0-2 [110]) with $R = 7.98$ Å; three with Mn-atoms being the fourth-nearest neighbors (0-1 [310], 0-1 $[3\bar{1}0]$, 0-1 $[5\bar{1}0]$), $R = 8.73$ Å, $R = 8.92$ Å, $R = 9.12$ Å, respectively; and one with Mn atoms being the fifth-nearest neighbors (0-2 [100]), $R = 11.29$ Å.

Having defined 11 configurations of the Mn pairs placed onto the 4×4 lateral unit cell, we are now in the position to determine their relative energetic stability. We define the incorporation energy of the Mn pair at the surface in configuration 0-n $[kl0]$ employing the standard expression [35]:

$$E_{\text{incorp}}(0\text{-}n\ [kl0]) := E_{\text{tot}}^{\text{slab,Mn-pair}}(0\text{-}n\ [kl0]) - E_{\text{tot}}^{\text{slab,pure}} - (\mu_{\text{Mn}} - \mu_{\text{Ga}})N_{\text{Mn}}, \quad (1)$$

where N_{Mn} is the number of Mn ions substituted on the Ga sites (N_{Mn} is always 2 in our studies), and μ_{Mn}, μ_{Ga} are the chemical potentials of Mn and Ga ions, respectively. However, since the number of substituted atoms in each considered configuration is identical, it is sufficient to consider only the total energy of the slab with the 0-n $[kl0]$ Mn pair normalized to the total energy of the pure slab:

$$\Delta E(0\text{-}n\ [kl0]) := E_{\text{tot}}^{\text{slab,Mn-pair}}(0\text{-}n\ [kl0]) - E_{\text{tot}}^{\text{slab,pure}}. \quad (2)$$

The values of this energy for some of the considered configurations 0-n $[kl0]$ versus the distance between the Mn atoms are depicted in Fig. 3(b). It is clearly seen that the energetically most stable configuration of the Mn pair on the (2×1) reconstructed (001) GaAs surface is the configuration with the Mn pair placed along the [110] direction with Mn atoms being the first neighbors on the cationic sublattice. Even then, the distance between Mn atoms in the 0-1 $[1\bar{1}0]$ configuration is smaller than in the 0-1 [110] one. This demonstrates the directional preference of accommodating the Mn pair on the (2×1) reconstructed surface, which results from the local environment of the Mn pair. However, as expected and seen in Fig. 3(b), the configurations with Mn atoms being farther apart are generally energetically less favorable. This is strong indication of the tendency of Mn atoms deposited on the surface to form pairs.

The energy difference between 0-1 [110] and 0-1 $[1\bar{1}0]$ configurations of the Mn-NN pair is 0.4 eV per supercell with 288 atoms. It is obvious that the local changes of the geometry contribute considerably to the relative stability of these two

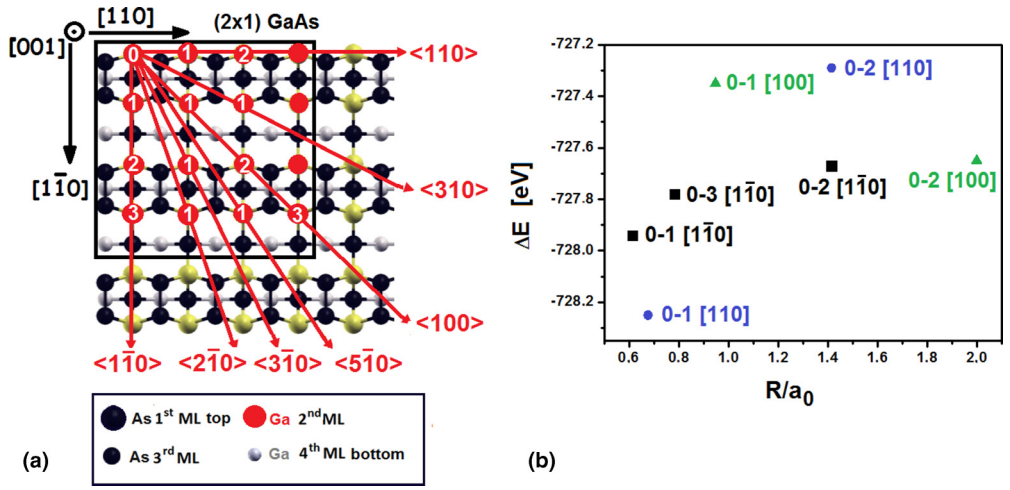

FIG. 3. (a) All nonequivalent positions of the Mn pair on the (2×1) reconstructed (001) surface. The two Mn atoms, replacing Ga atoms (red spheres), are marked 0 (first Mn atom) and 1,2,3 (second Mn atom); e.g., 0-3 [1$\bar{1}$0] denotes that the Mn pair is along the [1$\bar{1}$0] crystallographic direction, where Mn atoms constituting the pair sit on the 0 and 3 position as is depicted in panel (a). Note that the position 0-3 [1$\bar{1}$0] is equivalent to position 1-2 [1$\bar{1}$0] in a supercell, and so forth. All equivalent symmetry directions $\langle \dots \rangle$ have been chosen in direct cubic coordinates $[\dots]$, in such a way that all Mn pairs appear in the (001) plane. Positions of the atoms in the uppermost monolayers are indicated by larger symbols. Positions of the As atoms are denoted with big black dots. Small gray dots indicate the positions of the Ga atoms. (b) The stability of systems with the Mn pair incorporated into the (2×1) reconstructed surface, measured as the LDA energy differences $\Delta E = E_{\text{tot}}^{\text{slab,Mn-pair}}(MS) - E_{\text{tot}}^{\text{slab,pure}}$ as a function of the Mn-Mn distance. For clarity, the energetically less stable configurations [defined in panel (a)] have been omitted here. The two most stable configurations are the ones with Mn atoms being nearest neighbors along the [110] and [1$\bar{1}$0] directions.

configurations. It is worth pointing out now that when we place the Mn-NN pair along the [110] crystallographic direction, the symmetry is lowered to C_v in comparison to pure (2×1) reconstructed (001) GaAs surface (where it is C_{2v}), whereas the Mn-NN pair placed along the [1$\bar{1}$0] direction does not change the symmetry of the layer. As a consequence, we have noticed stronger relaxation of the atoms around the Mn-NN pair along the [110] direction than for the Mn pair along the [1$\bar{1}$0] direction.

All the results concerning relative stability of Mn pairs described above have been obtained employing standard nonmagnetic calculations with the LDA exchange-correlation functional. It is apparent that the change of the energy owing to the local rearrangement of atoms in the neighborhood of the Mn pair is roughly of the order of the magnetic energy of the Mn pair. Therefore, we included the magnetic interaction into our study employing the standard local spin density approximation [L(S)DA] and L(S)DA+U calculations. Employing these two methods, we consider parallel (ferromagnetic, FM) and antiparallel (antiferromagnetic, AFM) ordering of localized magnetic moments of Mn atoms constituting the Mn pair on the nearest-neighbor cationic positions along the [110] and [1$\bar{1}$0] directions. We use the standard value of $U = 4.5$ eV parameter for Mn atom that has been routinely used in many calculations involving Mn [12,24,25]. For nonoptimized atomic positions [36] around the Mn pair, the AFM ordering of Mn magnetic moments in the Mn pair is more favorable than the FM one for the [1$\bar{1}$0] direction, whereas for the Mn pair along the [110] direction the relation is reversed. The full relaxation of the slab does not change this picture as illustrated in Fig. 4. Qualitatively the same picture is obtained for both L(S)DA and L(S)DA+U functionals. From the point of view of magnetic interaction between the Mn atoms, the chemical arrangement of atoms around the Mn pair plays the crucial role, whereas the small changes of atomic geometry resulting from the relaxation of atomic positions has a negligible influence on it. In other words, only the chemical arrangement is able to change the direction of the magnetic moments on the Mn atoms, and hence the magnetic state (FM or AFM) of the (Ga,Mn)As system. For

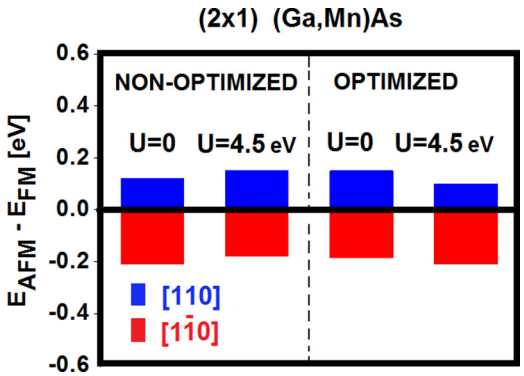

FIG. 4. The energy difference between AFM and FM Mn-spin alignment $E_{AFM} - E_{FM}$ in units of eV/supercell, for the nearest-neighbor 0-1 Mn pair along the [1$\bar{1}$0] (red) and [110] (blue) directions at the (2×1) reconstructed surface, as calculated within standard L(S)DA (indicated by $U = 0$) and L(S)DA+U (indicated by the used $U = 4.5$ eV value) methods. For the Mn-NN pair along the [1$\bar{1}$0] direction, the magnetic ground state is antiferromagnetic (AFM), whereas for the [110] direction, it is ferromagnetic (FM). It is seen that optimization of atomic positions does not change the magnetic state of the system.

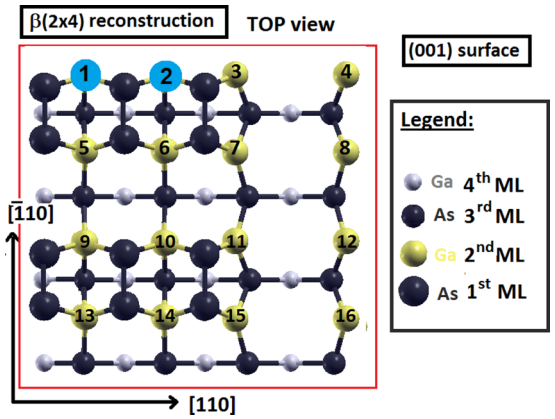

FIG. 5. Positions of Mn pairs at the $\beta(2 \times 4)$ reconstructed surface. The energetically most favorable position is for the Mn pair indicated as 1 & 2 along the [110] direction with FM ordering of spins. For emphasis, this pair is indicated by the blue color. This is true for both L(S)DA and L(S)DA+U calculations. All other cationic positions where Mn atoms can be substituted are indicated by yellow color and numbered 3-16. Note that 5 & 6 positions of Mn atoms are equivalent to 1 & 2 and lead to the same energy. Positions of the As atoms are indicated with big and small black dots for the highest and deeper As layers, respectively.

the L(S)DA+U method, the energies defined in Eq. (2) are as follows: ΔE(0-1 [110]; FM) $= -735.90$ eV; ΔE(0-1 [110]; AFM) $= -735.81$ eV; ΔE(0-1 [1$\bar{1}$0]; AFM) $= -735.54$; ΔE(0-1 [1$\bar{1}$0]; FM) $= -735.34$ eV. Therefore, the most stable configuration of the Mn pair incorporated into the (2×1) reconstructed (001) GaAs surface is 0-1 [110] with parallel magnetic moments of two Mn atoms.

The discussion for the (2×1) reconstructed surface sheds light on the energetics of the Mn pair incorporation at this surface. It clearly demonstrates the interplay between the magnetic interactions of the Mn atoms and atomic relaxations around them. Further, we follow the discussion for Mn pairs incorporated into $\beta(2 \times 4)$ and $\beta 2(2 \times 4)$ reconstructed surfaces. However, in light of the results obtained for the (2×1) reconstructed surface, we focus the discussion on Mn-NN pairs placed along the [110] and [1$\bar{1}$0] crystallographic directions.

2. *Reconstruction* $\beta(2 \times 4)$

We start the discussion with a survey of possible placements of the Mn-NN pairs on the $\beta(2 \times 4)$ (001) GaAs surface (see Fig. 5). In the chosen supercell of C_{2v} symmetry, the [110] and [1$\bar{1}$0] directions are nonequivalent. Along each of these directions, we can place the nearest-neighbor Mn pair on four equivalent ways on the cationic sublattice. They are 1 & 2, 5 & 6, 9 & 10, 13 & 14 for the [110], and 1 & 5, 2 & 6, 9 & 13, 10 & 14 for the [1$\bar{1}$0] direction.

However, along the [110] and [1$\bar{1}$0] directions we can place Mn nearest-neighbor pairs also in nonequivalent positions, such as 1 & 2, 2 & 3, 3 & 4, along [110], and 6 & 10, 7 & 11, 10 & 14, 11 & 15 along [1$\bar{1}$0]. The difference in energy for the nearest-neighbor (NN) configurations mostly stems from the fact that the surroundings of Mn-NN pairs are different, but also to a lesser extent, that the distance (after relaxation of atoms) between the Mn atoms constituting the pair also has been changed.

TABLE I. The stability of the systems with the incorporated Mn-NN pairs at the $\beta(2 \times 4)$ reconstructed (001) GaAs surface measured by the energy $\Delta E = E_{\text{tot}}^{\text{slab,Mn}}(MS) - E_{\text{tot}}^{\text{slab,pure}}$, given in units of eV/supercell. The Mn-pair positions are explained in Fig. 5. $E_{\text{tot}}^{\text{slab,pure}} = -39813.12$ eV/supercell with 284 atoms. The parallel and antiparallel spin alignment of the Mn-NN pair is indicated by FM and AFM, respectively. The results are obtained employing standard L(S)DA and L(S)DA+U ($U = 4.5$ eV) approaches.

$\beta(2 \times 4)$	$\Delta E_{L(S)DA}$ (eV/cell)		$\Delta E_{L(S)DA+U}$ (eV/cell)	
Mn-NN-pair position	FM	AFM	FM	AFM
[110] 1 & 2	−737.743	−737.448	−743.792	−743.555
[110] 2 & 3	−737.582	−737.456	−743.765	−743.666
[110] 3 & 4	−737.561	−737.413	−743.756	−743.636
[1$\bar{1}$0] 6 & 10	−737.415	−737.455	−743.521	−743.582
[1$\bar{1}$0] 7 & 11	−737.095	−737.053	−743.443	−743.430
[1$\bar{1}$0] 10 & 14	−737.539	−737.557	−743.627	−743.623
[1$\bar{1}$0] 11 & 15	−737.195	−737.318	−743.605	−743.697

From Fig. 5, one can also deduce the positions of the Mn pairs with longer than nearest-neighbor distances between Mn atoms. We have performed calculations for all nonequivalent positions of the Mn pairs. It turns out that the pairs with Mn atoms being the nearest neighbors are energetically preferable in comparison to the configurations with larger distances between the Mn atoms.

However, the relative energy differences among this class of configurations are dependent on the alignment of magnetic moments of the Mn-atoms (FM or AFM). This is illustrated in Table I, where the difference of the total energies of the slab with the Mn-NN pair and the pure slab (i.e., without the Mn-NN pair) is given for the L(S)DA and L(S)DA+U method.

Note that the total energy of the pure slab can be considered as a reference energy. This energy is identical for the L(S)DA and L(S)DA+U cases, since for the atoms in the pure slab (As, Ga, H) the Hubbard term U has been always taken as zero.

The energies of all nonequivalent Mn-pair arrangements (with Mn atoms being the nearest neighbors) are presented in Table I.

Among the Mn-NN pairs placed along the [110] direction, the lowest total energy is for FM Mn-spin arrangements and the Mn-NN pairs 1 & 2 (see Fig. 5, where this pair is indicated in blue). This is true for both L(S)DA and L(S)DA+U approaches. Among all Mn-NN pairs placed along the [1$\bar{1}$0] direction, the lowest total energy is for the AFM spin configuration for the Mn-NN-pair 10 & 14 in the L(S)DA approach (see Fig. 5) and for the Mn-NN pair 11 & 15 when the L(S)DA+U approach is employed. Generally, the L(S)DA and L(S)DA+U approaches lead to identical trends concerning the interplay between magnetic ordering and local environment of Mn-NN pairs. For all Mn-NN pairs along the [110] direction, the FM alignment of Mn spins is favorable over the AFM one. For Mn-NN pairs along the [1$\bar{1}$0] directions, generally the AFM spin alignment leads to lower energies than the FM one; however it is not the case for the Mn-NN pair numbered 7 & 11.

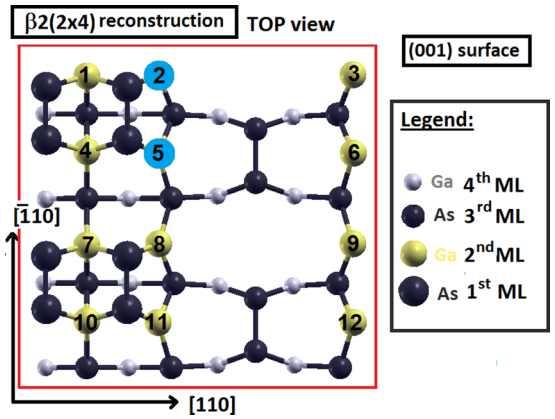

FIG. 6. Positions of Mn pairs at the $\beta 2(2 \times 4)$ reconstructed surface. According to the L(S)DA+U approach, the energetically most favorable configuration is the one with the Mn-NN pair (indicated as 2 & 5) along the $[1\bar{1}0]$ direction with AFM ordering of spins. This configuration has been indicated by blue color. All other possible positions of Mn atoms on the cationic sublattice are indicated by yellow color and numbered 3-12. Positions of the As atoms are indicated with big and small black dots for the highest and deeper As layers, respectively.

3. *Reconstruction* $\beta 2(2 \times 4)$

We discuss now structural and energetic properties of the Mn-NN pairs on the cationic sublattice and placed onto the $\beta 2(2 \times 4)$ reconstructed (001) surface.

As in the $\beta(2 \times 4)$ case, we start the discussion with a survey of possible placements of the Mn-NN pairs onto the $\beta 2(2 \times 4)$ (001) GaAs surface (see Fig. 6). In the chosen symmetry of the supercell, the [110] and $[1\bar{1}0]$ directions are nonequivalent. Along the [110] crystallographic direction, one can place the nearest-neighbor Mn pair in eight equivalent ways on the cationic sublattice, 1 & 2, 4 & 5, 7 & 8, 10 & 11, 1 & 3, 4 & 6, 7 & 9, and 10 & 12, which results in one class of nonequivalent positions represented by 1 & 2. Along the $[1\bar{1}0]$ direction, there are four classes of nonequivalent positions of the Mn-NN pair. They were chosen to be 1 & 4, 2 & 5, 4 & 7, and 5 & 8. Note that 1 & 4 and 7 & 10 or 5 & 8 and 6 & 9 are equivalent. Our results show that the pairs with Mn atoms being the nearest neighbors are energetically preferable in comparison to the configurations with larger distances between the Mn atoms. In Table II, we present the relative energy differences among all nearest-neighbor classes of Mn-pair configurations for FM and AFM alignments of magnetic moments of the Mn-NN pair.

The analysis of energies presented in Table II reveals the following picture. For the Mn-NN pair along the [110] direction, the FM alignment of spins is energetically more favorable than the AFM one [in both the L(S)DA and L(S)DA+U approaches], as was observed for the $\beta(2 \times 4)$ reconstruction. However this configuration [in contrast to the case of the $\beta(2 \times 4)$ reconstruction] is not the most stable one. The most stable configurations are observed for Mn-NN pairs along $[1\bar{1}0]$ directions. According to the standard L(S)DA the most stable configuration is the one with Mn atoms 4 & 7 along $[1\bar{1}0]$ with AFM Mn-spin alignment, whereas the L(S)DA+U predicts the 2 & 5 pair (indicated by blue color in Fig. 6) with AFM spin alignment to be the most energetically favorable.

TABLE II. The stability of the systems with the incorporated Mn-NN pairs at the $\beta 2(2 \times 4)$ reconstructed (001) GaAs surface measured by the energy $\Delta E = E_{\text{tot}}^{\text{slab,Mn}}(MS) - E_{\text{tot}}^{\text{slab,pure}}$, given in units of eV/supercell. The Mn-pair positions are explained in Fig. 6. $E_{\text{tot}}^{\text{slab,pure}} = -38570.17$ eV/supercell with 274 atoms. The parallel and antiparallel spin alignment of the Mn-NN pair is indicated by FM and AFM, respectively. The results are obtained employing standard L(S)DA and L(S)DA+U ($U = 4.5$ eV) approaches.

$\beta 2(2 \times 4)$	$\Delta E_{L(S)DA}$ (eV/cell)		$\Delta E_{L(S)DA+U}$ (eV/cell)	
Mn-NN-pair position	FM	AFM	FM	AFM
[110] (1 & 2)	−733.684	−733.483	−739.621	−739.465
$[1\bar{1}0]$ (1 & 4)	−733.825	−733.852	−739.601	−739.604
$[1\bar{1}0]$ (2 & 5)	−733.531	−733.571	−739.610	−739.693
$[1\bar{1}0]$ (4 & 7)	−733.855	−733.892	−739.614	−739.552
$[1\bar{1}0]$ (5 & 8)	−733.483	−733.386	−739.530	−739.459

However, one has to have in mind that the differences in energies of different configurations are extremely tiny.

4. *Comparison between different reconstructions*

In this section, we make an attempt to generalize our theoretical studies presented in the previous sections and gain a physical understanding of the structural and energetic properties of (001) GaAs surfaces incorporated with Mn pairs.

Our results show that the energy of the system strongly depends on the position, orientation, the distance between the Mn atoms, and relative alignment of Mn spins. The Mn pairs prefer to occupy the nearest-neighbor positions (NN) independently of the reconstruction type at the surface.

It turns out that for Mn-NN pairs there are two crystallographic orientations leading to the energetically most stable configurations, namely the [110] and $[1\bar{1}0]$ crystallographic directions. The energy differences between the most stable configurations along the $[1\bar{1}0]$ and [110] directions [as obtained within the L(S)DA and L(S)DA+U schemes] are summarized for all considered surface reconstructions in Fig. 7. One can

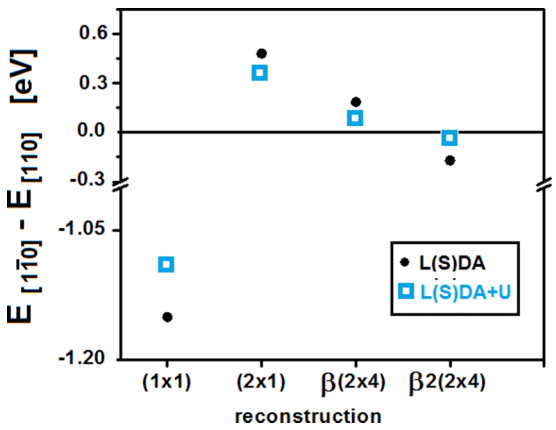

FIG. 7. Comparison of the most stable configurations of the Mn pairs at surfaces with various reconstructions. The energy difference between the most stable NN configuration at $[1\bar{1}0]$ and [110] crystallographic directions, as obtained within the L(S)DA and L(S)DA+U schemes.

see that the energetically preferential orientation of the Mn-NN pair depends on the surface reconstructions. In other words, it is plausible that during the growth process the Mn ions would accommodate positions along the energetically preferential directions. The very recent measurements have shown that there exist magnetic inhomogeneities on submillimeter length scales in (Ga,Mn)As samples [37], which can be assigned to anisotropic distribution of Mn-atom arrangements.

One of the important objectives of this study has been the investigation of the relation between the preferential distribution of the Mn pairs incorporated into the (001) GaAs surfaces and the origin of the uniaxial magnetic anisotropy in the (Ga,Mn)As samples, which, as was shown recently by the authors [4], can be ascribed to the breaking cubic symmetry of the bulk crystals by inhomogeneous distribution of Mn atoms [4]. Here we have shown that the energetically preferential positions of the Mn pairs depend on the surface reconstruction, and therefore, in principle, on the growth conditions. However, our static calculations cannot provide a direct hint on how the growth process leads to the predicted morphology of (001) GaAs surfaces with incorporated Mn pairs. To reach this goal molecular dynamics or kinetic Monte Carlo studies would be desirable, and this could be a challenging aim of future research. Nevertheless, our studies corroborate directly the existence of the preferential distribution of Mn pairs at the most important reconstructed (001) GaAs surfaces and also indirectly the plausibility that various distributions can be achieved by suitable growth conditions.

Finally we compare the stability of the pure surface with the stability of the just calculated surfaces with the incorporated Mn pairs, which could mimic the surfaces of (Ga,Mn)As. The stability of the structure can be determined by the standard thermodynamics, and have been well established for systems in equilibrium [38]. The most stable surface structure is determined by the minimum of the surface free energy γ, which is defined for a slab by the equation below [35,39]:

$$\gamma = \frac{1}{A}\left(E_{\text{surf}} - \sum_i \mu_i N_i\right), \tag{3}$$

where A is the surface area of the slab within the supercell, μ_i is the chemical potential of species i, and E_{surf} is the surface energy defined as

$$E_{\text{surf}} = \tfrac{1}{2}(E_{\text{slab}} - nE_{\text{bulk}}), \tag{4}$$

where E_{slab} denotes the total energy of the supercell, n is the number of bulk unit cells contained in the slab cell, and having energy E_{bulk}. In order to plot the surface free energy versus the thermodynamically allowed range of chemical potential, the surface free energy can be reexpressed as a function of the difference in the chemical potentials of the atomic As and As bulk, $\Delta\mu = \mu_{\text{As}} - \mu_{\text{As}}^{\text{bulk}}$. For the thermal equilibrium conditions [38,39], one obtains

$$\gamma = \frac{1}{A}\big[E_{\text{surf}} - N_{\text{Ga}}E_{\text{GaAs}}^{\text{bulk}} - N_{\text{Mn}}E_{\text{MnAs}}^{\text{bulk}} - \big(\mu_{\text{As}} - \mu_{\text{As}}^{\text{bulk}}\big)\Delta N - \mu_{\text{As}}^{\text{bulk}}\Delta N\big], \tag{5}$$

where the stoichiometry parameter is defined as $\Delta N = (N_{\text{As}} - N_{\text{Ga}} - N_{\text{Mn}})$, and $E_{\text{GaAs}}^{\text{bulk}}$ and $E_{\text{MnAs}}^{\text{bulk}}$ are the cohesive energies of GaAs and MnAs, respectively, when $T \to 0$ K. Our calculated heat of formation for MnAs is $\Delta H_f^{\text{MnAs}} = -0.52$ eV, and for GaAs is $\Delta H_f^{\text{GaAs}} = -0.73$ eV per unit cell with 2 atoms for both systems. The stoichiometry parameter ΔN determines the slope of the surface energy versus the difference in chemical potential $(\mu_{\text{As}} - \mu_{\text{As}}^{\text{bulk}})$. The stoichiometry parameter is defined by applying the method of Chetty and Martin [40], which utilizes the symmetry of the crystals and is the commonly used approach. For example, following counting method of Ref. [40], ΔN for the ideal (1×1) As-terminated surface is equal to $\frac{1}{2}$. In order to understand this counting rule one can think of a symmetric slab with two identical As-terminated surfaces. This slab has one As atom more than Ga across the slab, so there is $\frac{1}{2}$ additional As atom per (1×1) surface unit cell [39]. By this procedure, one obtains the stoichiometry parameter $\Delta N = \frac{1}{2}$ for (1×1) and (2×1) surfaces, and $\Delta N = \frac{1}{4}$ for $\beta(2 \times 4)$ and $\beta 2(2 \times 4)$ surfaces, where ΔN is counted per (1×1) lateral unit cell. Note that the lateral unit cell employed in the present studies is 16 times larger than the (1×1) unit cell, and therefore, the stoichiometry parameter takes the values $\Delta N = 8$ for (2×1) and $\Delta N = 4$ for $\beta(2 \times 4)$ and $\beta 2(2 \times 4)$ surface reconstructions.

The surface energies for the systems studied in this paper are presented in Fig. 8 for the L(S)DA approach. There, one can see that the pure $\beta 2(2 \times 4)$ reconstructed (001) GaAs surface is the most stable one for the whole range of chemical potentials. This is a consequence of the dimerization of the atoms at the surface, which reduces the numbers of dangling bonds and creates the sp^3-like bonds. The difference between the $\beta(2 \times 4)$ and $\beta 2(2 \times 4)$ surface energies is 4 meV/Å^2, which is the same order of magnitude as reported previously in the literature, where this difference was determined to lie in the range of 2–3 meV/Å^2 [7,41]. Moreover, one can see that all the reconstructions considered in Fig. 8 become more stable at the As-rich limit, i.e., $\mu_{\text{As}} - \mu_{\text{As}}^{\text{bulk}}$ approaching zero. The $\beta 2(2 \times 4)$ reconstructed surface with Mn-NN pair along the $[1\bar{1}0]$ direction is found to be energetically the most favorable of all Mn-reconstructed surfaces considered in this paper. The incorporation of the Mn-NN pair into the substitutional position for the $\beta(2 \times 4)$ and $\beta 2(2 \times 4)$ reconstructed surfaces stabilizes this surface by 5.4 meV/Å^2 and 4.6 meV/Å^2, respectively, whereas in the case of the (2×1) surface reconstruction, the effect is reversed and the surface is destabilized by 1.6 meV/Å^2.

B. Magnetic and electronic properties

In this section, we focus on the strength of the magnetic interaction of Mn-NN pairs at studied surfaces. Then we examine the electronic structure and spin magnetic moments.

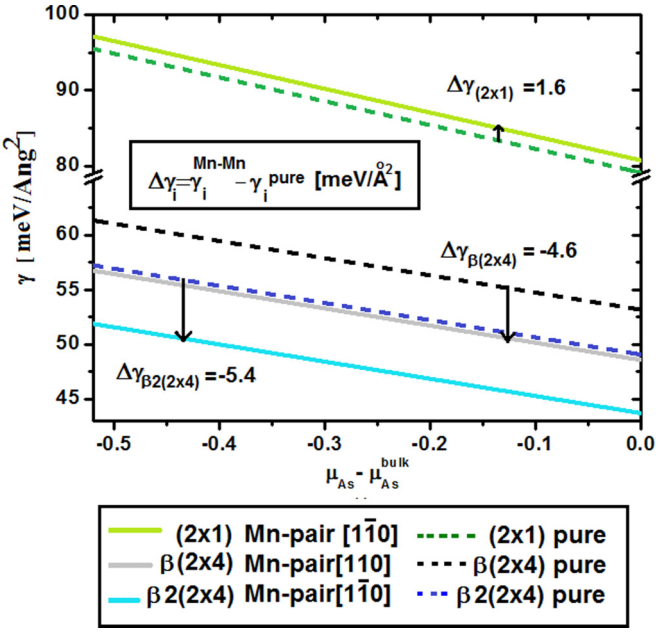

FIG. 8. Surface free energy diagrams for pure (001) GaAs, As-terminated surface reconstructions: (2 × 1), $\beta(2 \times 4)$, $\beta 2(2 \times 4)$ (denoted by the dashed lines), and for the most energetically preferable Mn-NN-pair substitutional incorporations onto these reconstructed surfaces (denoted by the straight lines) as predicted in this paper. The thermodynamically allowed range of the difference of chemical potentials of the As atom and As bulk is between −0.52 eV (Ga-rich conditions) and 0.00 eV (As-rich conditions). The arrows indicate the change in the surface free energy $\Delta\gamma_i$ owing to the incorporation of the Mn pair.

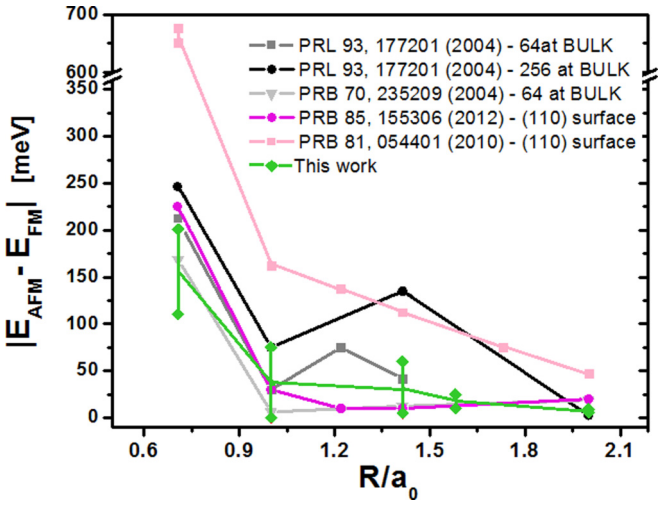

FIG. 9. The absolute value of the total energy difference between ferromagnetic and antiferromagnetic alignments of two Mn spins as a function of Mn-Mn separation (in lattice constant units a_0) for the surface and bulk calculations. The green line presents the result of this work for the surface reconstruction (2 × 1), and the green vertical lines indicate the obtained range of the magnetic energies for various nonequivalent Mn-pair configurations separation between the Mn ions. The internal panel shows the sources of data.

In order to show how the strength of the magnetic interaction of the Mn ions changes with the Mn-Mn distance, we plot the absolute value of energy difference between AFM and FM alignments of the magnetic moments of Mn atoms as a function of their separation (see Fig. 9). We assume collinear magnetic configurations of Mn ions in which magnetic moments are either parallel or antiparallel. We do not include spin-orbit interaction (SOI), because it has been reported recently that SOI has a small influence on exchange energy and on the exchange coupling constant J (a few meV) [14].

Since the exchange interaction is a crucial quantity in the field of DMS, we start our discussion comparing our results with the other theoretical predictions reported in the literature [12–14,37] (see Fig. 9), for both bulk and surface calculations obtained within different methods and different concentration of Mn ions. We would like to stress that the two older surface calculations [13,14] dealt with the nonpolar [110] GaAs surface that exhibits pronounced differences in comparison to the surfaces studied here.

The general trends of the exchange energy of the Mn pair at surfaces and in the bulk are similar, generally exhibiting a decay of the magnetic interaction with increasing distance between the magnetic ions.

As is clearly seen in Fig. 9, our results of the exchange energy are in the same range of energy as the rest of the DFT calculations depicted in this figure (for both bulk and surface). The largest discrepancy is for the tight-binding (T-B) calculations (see light pink curve with squared data points), for which the exchange energy values are approximately two times larger than energies obtained in DFT calculations. It is worth mentioning that our results for the exchange energy for the given distance between the Mn atoms constituting the pair are scattered within some energy range (indicated in Fig. 9 by bars) that is of order 100 meV for the nearest and second-nearest distances between Mn atoms. This is caused by the fact that at reconstructed surfaces the two Mn ions in a given distance between them can be placed in a series of nonequivalent ways. We would like to emphasize that the small energy difference of 13 meV (seen in Fig. 9) in the case of exchange energy obtained within the T-B calculations for the nearest distance between Mn atoms results from the SOI taken into account in the one of the T-B computations. This clearly demonstrates that the SOI effect on the exchange energy is an order of magnitude weaker than the environmental effect observed in our calculations and the neglect of SOI effects is justified for our purposes. In the following subsection, we present the detailed studies of the exchange coupling constants J which exhibit some kind of anisotropy, i.e., the dependence on the crystallographic direction along which the Mn pair is placed.

1. Effective exchange coupling

We have analyzed the effective exchange constant J for all the nonequivalent NN distances between the Mn ions at the reconstructed (001) GaAs surfaces: (2 × 1), $\beta(2 \times 4)$, and $\beta 2(2 \times 4)$ (see Table III), defined according to the formula $E_{AFM} - E_{FM} = 2JS^2$. Here, we assume the magnetic spins of Mn atoms to be $S = \frac{5}{2}$.

TABLE III. The exchange coupling J given in meV for the nearest-neighbor Mn pairs for various considered reconstructed surfaces. The numbers in brackets delimit the obtained range of the exchange coupling. The results are obtained employing standard L(S)DA and L(S)DA+U (for $U = 4.5$ eV) approaches.

	(2×1)	$\beta(2 \times 4)$	$\beta 2(2 \times 4)$
		Mn-Mn pair along [110]	
L(S)DA	+12	[+12,+24]	+16
L(S)DA+U	+7	[+8,+19]	+13
		Mn-Mn pair along $[1\bar{1}0]$	
L(S)DA	[−16,−13]	[−10,+4]	[−3,+8]
L(S)DA+U	[−18,−16]	[−7,+1]	[−7,+6]

Our results clearly demonstrate that the Mn-NN pair along the [110] crystallographic direction exhibits ferromagnetic alignment of spins, i.e., positive values of the exchange coupling J (see Table III), with magnetization vectors on each Mn atom being oriented along the [001] direction and of magnitude equal to 4.7 μ_B, independently of the type of reconstructed surface. For the Mn pair along the $[1\bar{1}0]$ crystallographic direction, the antiferromagnetic alignment of the spins is most likely to appear (mostly negative values of the exchange coupling J; see Table III). In other words, the mechanism of the magnetic ordering has the anisotropic character; namely, it depends on the Mn-pair orientation. This raises the question as to whether it would be possible (e.g., by the STM method) to incorporate on purpose the magnetic atoms along a given direction at the surface. Then one could obtain on purpose magnetic or nonmagnetic material. One can see that the value of the exchange constant for a given orientation of the Mn pair depends on the type of surface reconstruction, indicating that the exchange constant depends sensitively on the lattice arrangement of the atoms.

Now we compare our result with the exchange coupling for the pair reported so far in the literature. Those reports show that the effective J for the pair is highly sensitive to doping levels and increases with decreasing Mn concentration [12,15,37,42]. The order of magnitude of the exchange coupling calculated in our studies is the same as previously reported for the surface and bulk results. However, the bulk calculations always predict the ferromagnetic ordering of the Mn spins.

To our knowledge, previous surface calculations considered only the unreconstructed (110) nonpolar GaAs surface. The authors of Ref. [14] obtained, within the GGA approximation of DFT, a J value equal to 17.9 meV [43] for the nearest-neighbor configuration. Strandberg *et al.* [13] obtained positive values of J for two different directions of the Mn-NN pair at the (110) surface, 54 meV and 53 meV, for the very low Mn concentration of $x = 0.0006$. They used the kinetic tight-binding model. Due to the restrictions of the model they did not take into account relaxations of the atoms at the surface. This can significantly influence the results. Therefore, we believe that our studies provide reliable quantitative theoretical predictions and shed light on physical mechanisms leading to the magnetic structure of Mn pairs on the (001) GaAs surfaces. Further, we corroborate that the ordering mechanism of Mn spins is governed by the local environment of Mn atoms.

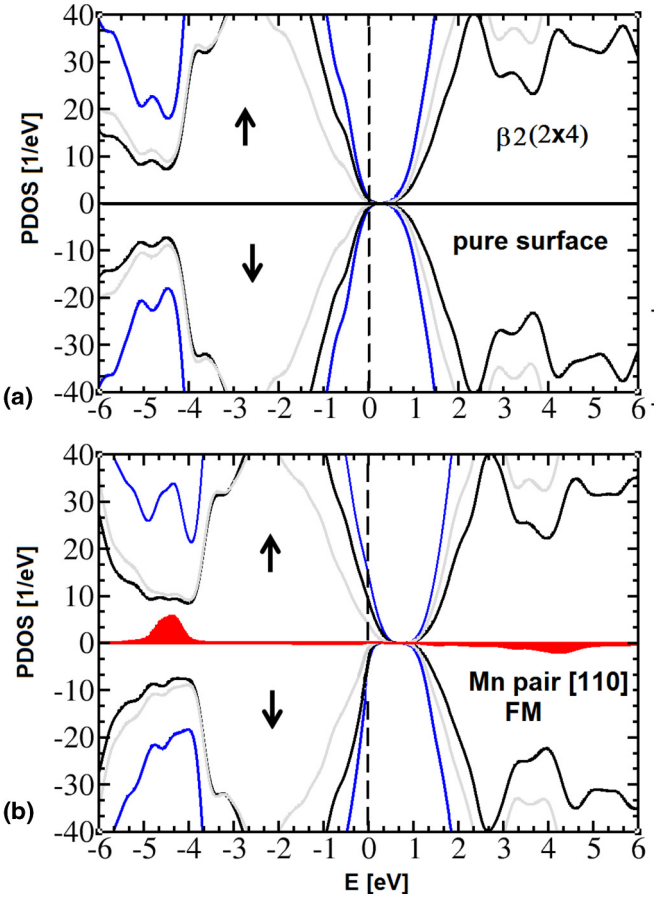

FIG. 10. Projected DOS calculated within L(S)DA+U method for (a) pure $\beta 2(2 \times 4)$ and (b) the Mn-NN pair substituted onto cationic sublattice along the [110] crystallographic direction at the $\beta 2(2 \times 4)$ surface. The pure $\beta 2(2 \times 4)$ surface is semiconducting, whereas substituted Mn ions introduce extra states above the Fermi level within the valence band. The vertical dashed line denotes the position of the Fermi level. The solid blue, black, and green lines correspond respectively to total density of all states in a system, total density of As states, and total density of Ga states. The red area is the contribution from Mn d states. The positive values of PDOS represent the spin-up channel, negative spin-down one.

2. *Electronic structure and spin magnetic moments*

Let us discuss now the changes of electronic structure caused by incorporation of the Mn-NN pair at the reconstructed (001) GaAs.

The pure (2×1) surface is metallic and the surface states are placed in the band gap of the bulk, whereas the pure β surfaces are semiconducting [see Fig. 10(a)] and do not introduce the surface states into the bulk's gap. Here, we focus on the electronic structure of the $\beta 2(2 \times 4)$ reconstructed surface with the incorporated Mn-NN pair. When the two Ga ions are substituted by the Mn ions, the extra electronic states appear just above the Fermi level [see Fig. 10(b)]. These empty states which are above the Fermi level and belong to the valence band can be identified with the hole states. As hole states, we consider unoccupied states with energies between the Fermi energy (lying in the valence band) [44] and the top of the valence band, as was previously considered for a bulk

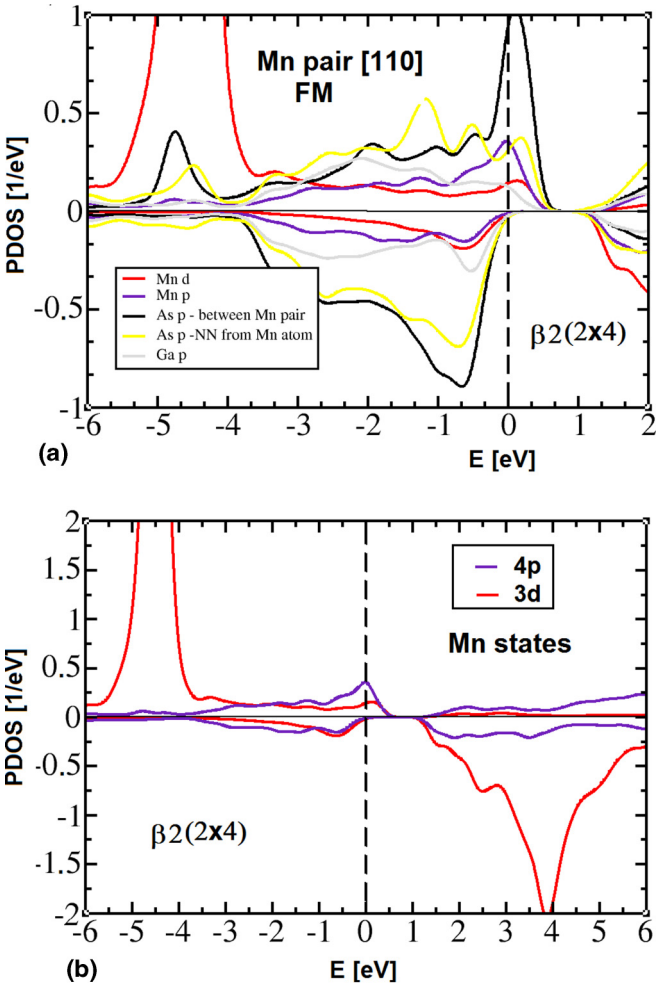

FIG. 11. PDOS as obtained from the L(S)DA+U calculations for the Mn-NN pair at the reconstructed $\beta 2(2 \times 4)$ surface. (a) Contribution of the surrounding atoms of the Mn-NN pair along the [110] crystallographic direction, and (b) the comparison between the Mn p and d states.

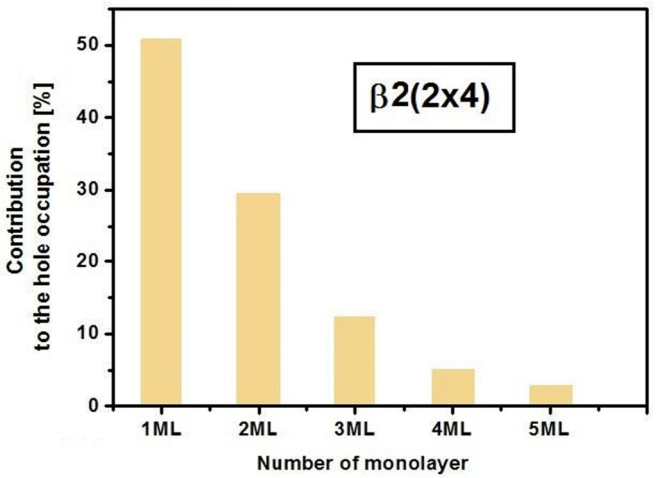

FIG. 12. Contribution (in %) to the hole occupation coming from various layers of the slab representing $\beta 2(2 \times 4)$ reconstructed (001) GaAs surface with incorporated Mn-NN pair along the [110] direction. 1ML indicates the top layer of As atoms; 2ML indicates the Ga atoms layer just below the top As layer. The Mn-NN pair is placed in this layer. 3ML and 5ML are As layers; 4ML is a Ga layer. The higher the number the deeper the position of the layer relative to the top one (1ML).

system [45,46]. The hole states have mostly p character [see Fig. 11(a)].

The greatest contribution to the holes comes from the arsenic atoms that are the nearest neighbors of the Mn-NN pair and reside along the [110] crystallographic direction [see Fig. 11(a)]. Moreover, the $3d$ states are mainly localized around 4.5 eV below the Fermi level [see Fig. 11(b)]. Therefore, the Mn p states hybridize with the surroundings stronger than the $3d$ states. There is only small admixture of the Mn d states with the hole states.

Now let us discuss the spatial distribution of the hole, in order to visualize its character. The hole occupation N_h is defined here as the integral over energy of the density of states from the Fermi energy to the top of the valence band. Note that the same procedure was previously adopted in Refs. [45] and [46] for the bulk system. One can also consider the integrated density of states $N_{h,\mathrm{layer}}$ coming from the projected DOS for various slab layers. The analysis of the contribution of the various layers to the total hole density (N_h) defined above is presented in Fig. 12 in the case of the $\beta 2(2 \times 4)$ reconstructed surface discussed here.

It is clearly seen that the contribution to the total hole occupancy decreases quickly with the depths of the layer, and the highest two layers (indicated as the 1ML and 2ML in Fig. 12) contribute 80% of the hole density. This result sheds light on the degree of the hole delocalization. We would like to emphasize that in our calculations no impurity band related to the surface acceptor has been observed. This clearly corresponds to the Zener type (or RKKY one) [47] of magnetic coupling between Mn ions, and the picture of surface, ligand-ion, p-d interaction is the adequate one.

The electronic structure of the $\beta(2 \times 4)$ reconstructed (001) GaAs surface with the Mn-NN pair with FM ordering of spins placed along the [110] direction is typical for other considered reconstructed (001) GaAs surfaces with incorporated Mn-NN pairs and exhibits all essential features. It is illustrated in Fig. 13(a). For comparison, in Fig. 13(b), we plot also the density of states for the Mn-NN pair with AFM spin ordering incorporated along the $[1\bar{1}0]$ direction into three types of the reconstructed GaAs (001) surfaces discussed in the present paper. With the discussion presented above, this figure is self-explanatory.

Now, let us focus on distribution of magnetic moments in the surroundings of the Mn-NN pair by using Mulliken analysis [48]. Our results clearly show that the local magnetic moments of Mn ions polarize their surroundings always in such a way that the nearest-neighbor As atoms acquire the magnetic moments antiferromagnetically aligned to the Mn spins, which is schematically illustrated in Fig. 14 for the case of the (2×1) reconstructed surface. For the Mn-NN pair along the [110] direction (i.e., with FM ordering of spins), the values of magnetic moments on As-atoms surrounding Mn ones are listed for three considered surface reconstructions in Table IV.

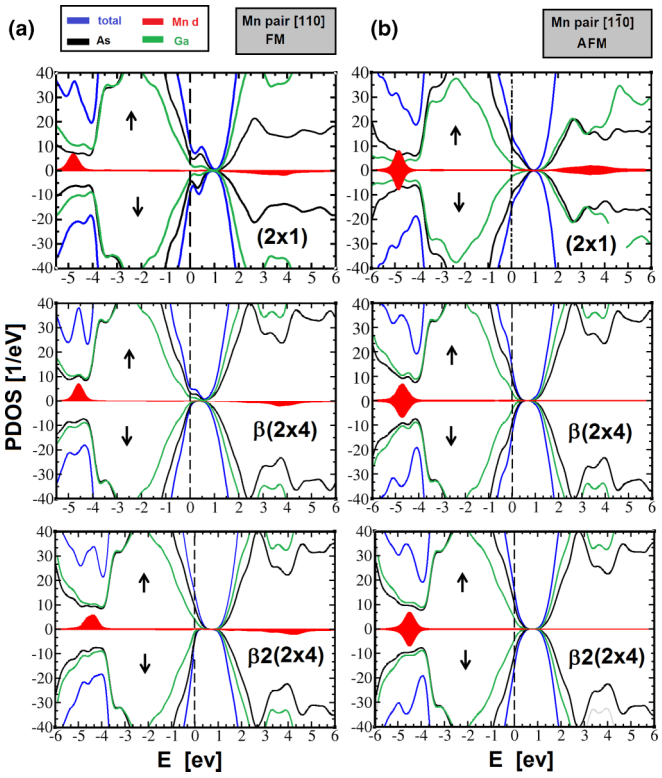

FIG. 13. PDOS calculated within L(S)DA+U method for the three reconstructed surfaces of GaAs with the Mn-NN pair along two different orientations: [110] (left side of the picture) and [1$\bar{1}$0] (right side of the picture). Spin alignments for Mn-NN pairs are FM and AFM, for direction [110] and [1$\bar{1}$0], respectively. The vertical dashed line denotes the position of the Fermi level. The solid blue, black, and green lines correspond respectively to total density of all states in a system, total density of As states, and total density of Ga states. The red area indicates the contribution from Mn d states.

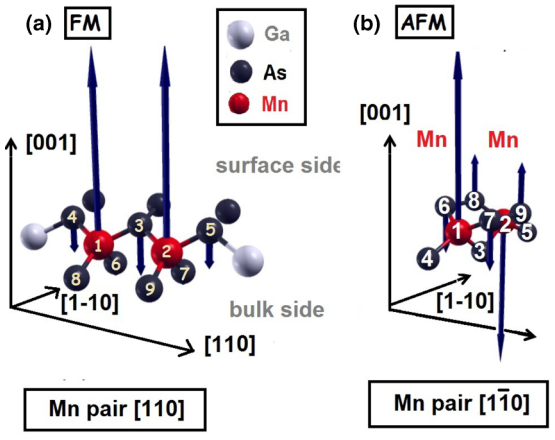

FIG. 14. Distribution of magnetic moments on As atoms surrounding the Mn-NN pair placed along [110] (a) and [1$\bar{1}$0] (b) crystallographic directions at the (2 × 1) reconstructed (001) GaAs surface. The blue arrows indicate the magnetic moments of Mn atoms with FM (a) and AFM (b) alignments. The lengths of the magnetic vectors on As sites are exaggerated for clarity of the presentation.

TABLE IV. The spin magnetic polarization (in units of μ_B/atom) of the As atoms surrounding Mn ions for the FM arrangement of the Mn-NN pair at the [110] direction for various reconstructed surfaces, as calculated by using Mulliken analysis [48]. The As atoms are numbered according to Fig. 14.

	Surface reconstruction		
atom	(2 × 1)	$\beta(2\times4)$	$\beta2(2\times4)$
As3	−0.74	−0.75	−0.79
As4	−0.2	−0.17	−0.2
As5	−0.2	−0.17	
As9 = As7	−0.12	−0.10	−0.17
As8 = As6	−0.12	−0.10	−0.09

One can see that the induced magnetic moments are comparable and do not depend on the type of reconstructed surfaces. They decrease rapidly with the increasing distance to the Mn pair. Only the nearest neighbors of the Mn pair have (i.e., these depicted in Fig. 14) noticeable induced spin polarization. For the second neighbors, the induced magnetic moments are smaller than 0.01 μ_B, and for the third neighbors, the magnetic moments are nearly equal to zero. The same picture emerges from both L(S)DA and L(S)DA+U calculations. In the bulk system, the magnetic moment on the first, second, and third Mn neighbor extends to 0.11 μ_B, 0.015 μ_B, and 0.015 μ_B, respectively (according to the L(S)DA+U [12]). This comparison between the bulk and the surface shows that the induced magnetic moments are more localized at the surface than in the bulk. In addition, the induced magnetic moments on the atoms are always larger at the surface than at the monolayer closer to the bulk site. In the case of AFM alignment of Mn spins, the As atom positioned between the Mn-NN pair is not spin polarized. Other As neighbors of Mn atoms have absolute values of spin polarization similar to those in the FM case.

IV. CONCLUSIONS

We have studied the stability, morphology, and electronic structure of Mn pairs substituted onto the Ga sublattice at different As-terminated reconstructed (001) GaAs surfaces. We have demonstrated that the energy of the system depends on the position, orientation, and distance between the Mn atoms. The Mn pairs with Mn atoms being the nearest neighbors (i.e., constituting Mn pair) are energetically the most favorable, independently of the surface reconstruction pattern. This causes that there are only two crystallographic directions, namely [110] and [1$\bar{1}$0], relevant for incorporation of the Mn-NN pair at the surface. For (2 × 1) and $\beta(2\times4)$ reconstruction patterns, the Mn-NN pair placed along the [110] direction is more stable than the Mn-NN pair placed along the [1$\bar{1}$0] direction. On the contrary, for (1 × 1) and $\beta2(2\times4)$ reconstructions, the energetically stable configuration of the system requires the Mn-NN pair along the [1$\bar{1}$0] direction. Our results point to the possibility of affecting the magnetic anisotropy of the (Ga,Mn)As layer [4] by forcing an alternative reconstruction of the semiconductor surface, during the growth, by choosing appropriate growth conditions—namely the vapor pressure,

temperature, or surface composition [49,50]. Moreover, we have demonstrated that the mechanism of the magnetic ordering depends on the Mn-NN-pair orientation. Generally, the Mn-NN pair along the [110] crystallographic direction exhibits ferromagnetic alignment of the spins, whereas the Mn-NN pair along the $[1\bar{1}0]$ crystallographic direction prefers to be antiferromagnetically aligned. In addition, we have shown that the Mn $4p$ states have greater contribution to the hole states than $3d$ states, which is consistent with recently published theoretical results for bulk (Ga,Mn)As [45,46].

We have demonstrated that the holes are mostly localized in the closest proximity of the Mn-NN pair. Nevertheless, there are small contributions which come from the distant atoms indicating extended character of the holes. These observations strongly suggest that the Zener p-d interaction [47] can also cause ferromagnetic coupling of the Mn-NN pairs at the surface, provided the magnetic moments of the Mn-atoms forming the pair do not cancel each other (FM configurations).

Furthermore, our results clearly show that the local magnetic moments of Mn ions polarize their surroundings always in such a way that the Mn nearest-neighbor As atoms acquire the magnetic moments which are antiferromagnetically aligned to the Mn spins.

ACKNOWLEDGMENTS

The authors are grateful to T. Dietl for illuminating discussions. This work was supported by the European Research Council through the FunDMS Advanced Grant within the "Ideas" Seventh Framework Programme of the EC and InTechFun (POIG.01.03.01-00-159/08) of EC. We made use of computing facilities of PL-Grid Polish Infrastructure for Supporting Computational Science in the European Research Space, and acknowledge the access to the computing facilities of the Interdisciplinary Centre of Modelling, University of Warsaw. The support of the National Research Council (NCN) through the grant HARMONIA DEC-2013/10/M/ST3/00793 is gratefully acknowledged.

[1] T. Dietl and H. Ohno, Dilute ferromagnetic semiconductors: Physics and spintronic structures, Rev. Mod. Phys. **86**, 187 (2014).

[2] T. Jungwirth, J. Wunderlich, V. Novák, K. Olejník, B. L. Gallagher, R. P. Campion, K. W. Edmonds, A. W. Rushforth, A. J. Ferguson, and P. Němec, Spin-dependent phenomena and device concepts explored in (Ga,Mn)As, Rev. Mod. Phys. **86**, 855 (2014).

[3] P. Mahadevan and A. Zunger, Ferromagnetism in Mn-doped GaAs due to substitutional-interstitial complexes, Phys. Rev. B **68**, 075202 (2003).

[4] M. Birowska, C. Śliwa, J. A. Majewski, and T. Dietl, Origin of Bulk Uniaxial Anisotropy in Zinc-Blende Dilute Magnetic Semiconductors, Phys. Rev. Lett. **108**, 237203 (2012).

[5] D. Chiba, M. Sawicki, Y. Nishitani, Y. Nakatani, F. Matsukura, and H. Ohno, Magnetization vector manipulation by electric fields, Nature (London) **455**, 515 (2008).

[6] D. Kitchen, A. Richardella, J.-M. Tang, M. E. Flatte, and A. Yazdani, Atom-by-atom substitution of Mn in GaAs and visualization of their hole-mediated interactions, Nature (London) **442**, 436 (2006).

[7] S. C. Erwin and A. G. Petukhov, Self-Compensation in Manganese-Doped Ferromagnetic Semiconductors, Phys. Rev. Lett. **89**, 227201 (2002).

[8] S. B. Zhang, L. Zhang, L. Xu, E. G. Wang, X. Liu, J.-F. Jia, and Q.-K. Xue, Spin driving reconstructions on the GaAs(001):Mn surface, Phys. Rev. B **69**, 121308 (2004).

[9] A. Ohtake, A. Hagiwara, and J. Nakamura, Controlled incorporation of Mn in GaAs: Role of surface reconstructions, Phys. Rev. B **87**, 165301 (2013).

[10] H. Fu, L. Ye, K. Zhang, and X. Xie, Chemisorption of Mn on a GaAs(110) surface, Surf. Sci. **341**, 273 (1995).

[11] S. L. Dudarev, G. A. Botton, S. Y. Savrasov, C. J. Humphreys, and A. P. Sutton, Electron-energy-loss spectra and the structural stability of nickel oxide: An LSDA+U study, Phys. Rev. B **57**, 1505 (1998).

[12] M. Wierzbowska, D. Sánchez-Portal, and S. Sanvito, Different origins of the ferromagnetic order in (Ga,Mn)As and (Ga,Mn)N, Phys. Rev. B **70**, 235209 (2004).

[13] T. O. Strandberg, C. M. Canali, and A. H. MacDonald, Magnetic interactions of substitutional Mn pairs in GaAs, Phys. Rev. B **81**, 054401 (2010).

[14] M. F. Islam and C. M. Canali, *Ab initio* calculations of the magnetic properties of Mn impurities on GaAs (110) surfaces, Phys. Rev. B **85**, 155306 (2012).

[15] M. van Schilfgaarde and O. N. Mryasov, Anomalous exchange interactions in III-V dilute magnetic semiconductors, Phys. Rev. B **63**, 233205 (2001).

[16] K. M. Yu, W. Walukiewicz, T. Wojtowicz, I. Kuryliszyn, X. Liu, Y. Sasaki, and J. K. Furdyna, Effect of the location of Mn sites in ferromagnetic $Ga_{1-x}Mn_xAs$ on its Curie temperature, Phys. Rev. B **65**, 201303 (2002).

[17] P. Hohenberg and W. Kohn, Inhomogeneous electron gas, Phys. Rev. **136**, B864 (1964).

[18] W. Kohn and L. J. Sham, Self-consistent equations including exchange and correlation effects, Phys. Rev. **140**, A1133 (1965).

[19] D. M. Ceperley and B. J. Alder, Ground State of the Electron Gas by a Stochastic Method, Phys. Rev. Lett. **45**, 566 (1980).

[20] P. Ordejón, E. Artacho, and J. M. Soler, Self-consistent order-N density-functional calculations for very large systems, Phys. Rev. B **53**, R10441 (1996).

[21] N. Troullier and J. L. Martins, Efficient pseudopotentials for plane-wave calculations, Phys. Rev. B **43**, 1993 (1991).

[22] S. G. Louie, S. Froyen, and M. L. Cohen, Nonlinear ionic pseudopotentials in spin-density-functional calculations, Phys. Rev. B **26**, 1738 (1982).

[23] E. Artacho, D. Sánchez-Portal, P. Ordejón, A. García, and J. M. Soler, Linear-scaling *ab initio* calculations for large and complex systems, Phys. Status Solidi (b) **215**, 809 (1999).

[24] J. Okabayashi, A. Kimura, O. Rader, T. Mizokawa, A. Fujimori, T. Hayashi, and M. Tanaka, Angle-resolved photoemission study of $Ga_{1-x}Mn_xAs$, Phys. Rev. B **64**, 125304 (2001).

[25] T. Jungwirth, J. Sinova, J. Maš, J. Kucera, and A. H. MacDonald, Theory of ferromagnetic (III,Mn)V semiconductors, Rev. Mod. Phys. **78**, 809 (2006).

[26] D. A. Murdick, X. W. Zhou, H. N. G. Wadley, and D. Nguyen-Manh, Predicting surface free energies with interatomic potentials and electron counting, J. Phys.: Condens. Matter **17**, 6123 (2005).

[27] O. Madelung, *Semiconductors: Data Handbook*, 3rd ed. (Springer, Berlin, 2004).

[28] M. D. Pashley, K. W. Haberern, W. Friday, J. M. Woodall, and P. D. Kirchner, Structure of GaAs(001) (2×4)-$c(2 \times 8)$ Determined by Scanning Tunneling Microscopy, Phys. Rev. Lett. **60**, 2176 (1988).

[29] E. J. Heller and M. G. Lagally, Insitu scanning tunneling microscopy observation of surface morphology of GaAs(001) grown by molecular beam epitaxy, Appl. Phys. Lett. **60**, 2675 (1992).

[30] M. Gallagher, R. Prince, and R. Willis, On the atomic structure and electronic properties of decapped GaAs(001) (2×4) surfaces, Surf. Sci. **275**, 31 (1992).

[31] A. Avery, D. Homes, J. Sudijono, T. Jones, and B. Joyce, The As-terminated reconstructions formed by GaAs(001): A scanning tunneling microscopy study of the (2×4) and $c(4 \times 4)$ surfaces, Surf. Sci. **323**, 91 (1995).

[32] M. Takahasi, Y. Yoneda, N. Yamamoto, and J. Mizuki, Domain boundaries in the GaAs(001)-(2×4) surface, Phys. Rev. B **68**, 085321 (2003).

[33] Experimentally, this reconstruction is observed on Si(001) surfaces.

[34] S. Colonna, E. Placidi, F. Ronci, A. Cricenti, F. Arciprete, and A. Balzarotti, The role of kinetics on the Mn-induced reconstructions of the GaAs(001) surface, J. Appl. Phys. **109**, 123522 (2011).

[35] F. Bechstedt, *Principles of Surface Physics* (Springer-Verlag, Berlin, 2003).

[36] "Nonoptimized atomic positions" refer to the ideal position of GaAs surface atoms. In other words, we have substituted the Ga atoms with the Mn atoms without allowing the atoms to relax.

[37] P. Mahadevan, A. Zunger, and D. D. Sarma, Unusual Directional Dependence of Exchange Energies in GaAs Diluted with Mn: Is the RKKY Description Relevant? Phys. Rev. Lett. **93**, 177201 (2004).

[38] G.-X. Qian, R. M. Martin, and D. J. Chadi, First-principles study of the atomic reconstructions and energies of Ga- and As-stabilized GaAs(100) surfaces, Phys. Rev. B **38**, 7649 (1988).

[39] A. Groß, *Theoretical Surface Science*, 2nd ed. (Springer, Berlin, 2009).

[40] N. Chetty and R. M. Martin, Determination of integrals at surfaces using the bulk crystal symmetry, Phys. Rev. B **44**, 5568 (1991).

[41] S.-H. Lee, W. Moritz, and M. Scheffler, GaAs(001) Surface under Conditions of Low As Pressure: Evidence for a Novel Surface Geometry, Phys. Rev. Lett. **85**, 3890 (2000).

[42] J. Kudrnovský, I. Turek, V. Drchal, F. Máca, P. Weinberger, and P. Bruno, Exchange interactions in III-V and group-IV diluted magnetic semiconductors, Phys. Rev. B **69**, 115208 (2004).

[43] See Table VII in Ref. [14]. For $U = 4$ eV, the value of the difference between the E_{AFM} and E_{FM} is equal to 223.7 meV. In order to obtain the exchange constant J, we normalized the values quoted in Ref. [14] dividing them by the factor $2 \times (5/2)^2 = 12.5$ (see the formula for the exchange coupling).

[44] We have not considered the holes in the system with Mn-NN pair on the (2×1) reconstructed surface. The reason is the appearance of the unoccupied surface states in the band gap for the pure (2×1) reconstruction, and their mixing with the unoccupied states coming from the substitution of the Mn atoms at the cationic sublattice.

[45] L. M. Sandratskii, P. Bruno, and J. Kudrnovský, On-site Coulomb interaction and the magnetism of (GaMn)N and (GaMn)As, Phys. Rev. B **69**, 195203 (2004).

[46] K. Z. Milowska and M. Wierzbowska, Hole sp^3 character and delocalization in (Ga,Mn)As revised with pSIC and MLWF approaches—newly found spin-unpolarized gap states of s-type below 1% of Mn, Chem. Phys. **430**, 7 (2014).

[47] T. Dietl, F. Matsukura, J. Cibert, and D. Ferrand, Zener model description of ferromagnetism in zinc-blende magnetic semiconductors, Science **287**, 1019 (2000).

[48] R. S. Mulliken, Electronic population analysis on LCAOMO molecular wave functions, J. Chem. Phys. **23**, 1833 (1955).

[49] H. Shimizu, T. Hayashi, T. Nishinaga, and M. Tanaka, Magnetic and transport properties of III-V based magnetic semiconductor (Ga,Mn)As: Growth condition dependence, Appl. Phys. Lett. **74**, 398 (1999).

[50] G. M. Schott, W. Faschinger, and L. W. Molenkamp, Lattice constant variation and complex formation in zinc-blende gallium manganese arsenide, Appl. Phys. Lett. **79**, 1807 (2001).